



**HAL**  
open science

## **Contribution of deep soil layers to the transpiration of a temperate deciduous forest: Implications for the modelling of productivity**

Jean Maysonnave, Nicolas Delpierre, Christophe François, Marion Jourdan, Ivan Cornut, Stéphane Bazot, Gaëlle Vincent, Alexandre Morfin, Daniel Berveiller

### ► To cite this version:

Jean Maysonnave, Nicolas Delpierre, Christophe François, Marion Jourdan, Ivan Cornut, et al.. Contribution of deep soil layers to the transpiration of a temperate deciduous forest: Implications for the modelling of productivity. *Science of the Total Environment*, 2022, 838 (Part 2), pp.155981. 10.1016/j.scitotenv.2022.155981 . hal-03857864

**HAL Id: hal-03857864**

**<https://hal.science/hal-03857864>**

Submitted on 17 Nov 2022

**HAL** is a multi-disciplinary open access archive for the deposit and dissemination of scientific research documents, whether they are published or not. The documents may come from teaching and research institutions in France or abroad, or from public or private research centers.

L'archive ouverte pluridisciplinaire **HAL**, est destinée au dépôt et à la diffusion de documents scientifiques de niveau recherche, publiés ou non, émanant des établissements d'enseignement et de recherche français ou étrangers, des laboratoires publics ou privés.

# Contribution of deep soil layers to the transpiration of a temperate deciduous forest: quantification and implications for the modelling of productivity

Jean Maysonnave<sup>1,+</sup>, Nicolas Delpierre<sup>1,2,+,\*</sup>, Christophe François<sup>1</sup>, Marion Jourdan<sup>1</sup>, Ivan Cornut<sup>1,3</sup>, Stéphane Bazot<sup>1</sup>, Gaëlle Vincent<sup>1</sup>, Alexandre Morfin<sup>1</sup>, Daniel Berveiller<sup>1</sup>

<sup>1</sup>Université Paris-Saclay, CNRS, AgroParisTech, Ecologie Systématique et Evolution, 91405, Orsay, France.

<sup>2</sup>Institut Universitaire de France (IUF)

<sup>3</sup>CIRAD, UMR Eco&Sols, F-34398 Montpellier, France

\*Corresponding author: nicolas.delpierre@universite-paris-saclay.fr

<sup>+</sup>both authors contributed equally

## 1 Abstract

2 Climate change is imposing drier atmospheric and edaphic conditions on temperate forests.  
3 Here, we investigated how deep soil (down to 300 cm) water extraction contributed to the pro-  
4 vision of water in the Fontainebleau-Barbeau temperate oak forest over two years, including the  
5 2018 record drought. Deep water provision was key to sustain canopy transpiration during drought,  
6 with layers below 150 cm contributing up to 60% of the transpired water in August 2018, despite  
7 their very low density of fine roots. We further showed that soil databases used to parameter-  
8 ize ecosystem models largely underestimated the amount of water extractable from the soil by  
9 trees, due to a considerable underestimation of the tree rooting depth. The consensus database  
10 established for France gave an estimate of 207 mm for the soil water holding capacity (SWHC) at  
11 Fontainebleau-Barbeau, when our estimate based on the analysis of soil water content measure-  
12 ments was 1.9 times as high, reaching  $390 \pm 17$  mm. Running the CASTANEA forest model with  
13 the database-derived SWHC yielded a  $350 \text{ gC m}^{-2} \text{ y}^{-1}$  average underestimation of annual gross  
14 primary productivity under current climate, reaching up to  $700 \text{ gC m}^{-2} \text{ y}^{-1}$  under climate change  
15 scenario RCP8.5. It is likely that the strong underestimation of SWHC that we show at our site is  
16 not a special case, and concerns a large number of forest sites. Thus, we argue for a generalisation

17 of deep soil water content measurements in forests, in order to improve the estimation of SWHC  
18 and the simulation of the forest carbon cycle in the current context of climate change.

## 19 **Keywords**

20 water uptake, deep soil, water stress, soil water holding capacity, carbon fluxes, gross primary  
21 productivity, temperate oaks

## 22 **Highlights**

- 23 • Forest-atmosphere carbon exchanges remained insensitive to record drought.
- 24 • Deep soil (150-300 cm) provisioned up to 60% of the water transpired by the forest during  
25 drought.
- 26 • Soil databases were underestimating soil water holding capacity by a factor of two.
- 27 • Simulated forest productivity is strongly sensitive to soil water holding capacity parameter.
- 28 • Deep soil water content measurements are urgently needed to correctly estimate the soil  
29 water holding capacity.

## 30 **Introduction**

31 Evaporating water is vital for trees. The process of evapotranspiration plays a central role in  
32 the thermoregulation of leaves, the acquisition and transport of nutrients from the soil to plant  
33 organs and is an inescapable consequence of the stomatal opening for the acquisition of carbon from  
34 the atmosphere. In plant communities, orders of magnitude for the amount of water transpired  
35 per unit carbon gained through photosynthesis range from 190 grams of water per unit gram of  
36 carbon as a global estimate for terrestrial vegetation (Cramer et al., 2009) to 330 g(H<sub>2</sub>O)/g(C) in  
37 the FLUXNET database (Baldocchi and Peñuelas, 2019). This means that considerable amounts  
38 of water are necessary for sustaining the basic functioning of plant communities, and particularly  
39 of forests which can grow high leaf areas (Asner et al., 2003) leading to high evapotranspiration  
40 fluxes. Being sessile organisms, plants rely on the soil stores to provide this water resource. Since  
41 the amount of water stored in the soil and accessible to plants is generally lower than the amount  
42 of water that could be evaporated considering the local energy balance, plant communities have  
43 evolved a range of controls of the water loss to the atmosphere from the scale of the leaf (i.e.  
44 stomatal closure; Martin-StPaul et al., 2017) to the canopy (i.e. control of the leaf area index;  
45 Eagleson, 1982). More generally, the modification of a large range of physiological processes  
46 (Hsiao et al., 1976) along the depletion of the plant water potential illustrates the adaptation of  
47 plants to water shortage. Located at both ends of the soil-plant-atmosphere water continuum, the  
48 atmospheric demand for water vapor (that relates to vapor pressure deficit, VPD), and the capillary  
49 forces retaining water molecules in the soil impose a tension on the water-column ascending the  
50 plant xylem. Increases in the atmospheric demand and/or the tension of water in the plant result in  
51 progressive stomatal closure (Martin-StPaul et al., 2017) that tends to mitigate the water potential  
52 drop-down and prevent xylem embolism.

53 Characterising the response of the canopy to VPD is rather straightforward (Oren et al., 1999;  
54 Novick et al., 2016; Grossiord et al., 2020) since atmospheric VPD can readily be measured, or  
55 calculated from measurements of relative humidity and temperature. On the other hand, the role  
56 of soil moisture in controlling canopy gas exchanges has remained more difficult to quantify. Soil  
57 matric potential (in MPa), which would be the physical measurement most relevant to quantify

58 the soil water availability to the plants, is rarely measured. Instead, soil water content (SWC,  
59 in  $\text{m}^3_{\text{water}} \text{m}^{-3}_{\text{soil}}$ ) is usually monitored, and then possibly interpreted as water potential through  
60 pressure-volume functions (e.g. van Genuchten, 1980). Even then, SWC is usually measured over  
61 shallow soil depths for practical reasons (typically down to 20-50 cm, see e.g. Granier et al., 2007;  
62 Novick et al., 2016), which in many cases is not suitable for quantifying the total stock of water  
63 available to trees. Indeed, trees often grow roots deep in the soil, down to several meters (Fan et al.,  
64 2017), which can be essential for provisioning the water needed for transpiration and the overall  
65 tree functioning during periods of water shortage (Germon et al., 2020; Christina et al., 2017;  
66 McCormick et al., 2021) even if representing a small fraction of the root system mass (Jackson  
67 et al., 1996). Specifically in oaks, Lucot and Bruckert (1992) documented the presence of fine roots  
68 down to 4 meters in a *Quercus robur* plot with no physical or chemical constraints. Bréda et al.  
69 (1995) reported both the presence of fine roots and water extraction down to 2-meters in *Quercus*  
70 *petraea*.

71 Reflecting this "shallow-soil bias", models of ecosystem functioning have so far mostly con-  
72 sidered soil water to be extractable only in the upper horizons of the soil, defining the so-called  
73 "soil water holding capacity" (SWHC, the amount of water, in millimeters, extractable from the  
74 soil by plants) at typical depths of one to two meters (e.g. Piedallu et al., 2011; Krinner et al.,  
75 2005; Dufrène et al., 2005; Granier et al., 2007). This parameter has been shown very sensitive in  
76 the modelling of ecosystem water balance (Granier et al., 1999), carbon balance (Dufrène et al.,  
77 2005), tree growth (Guillemot et al., 2017) and survival (Cheaib et al., 2012; Preisler et al., 2019).  
78 Challenging the SWHC concept, and in accordance with the recognition of deep water as essential  
79 for the functioning of trees, recent works have defined the Total Available Water (TAW) concept,  
80 that adds "deep water" extraction by trees to SWHC considered over 1-m (Carrière et al., 2020).  
81 However, this deep water resource remains poorly quantified because the trees actual rooting depth  
82 and the capacity of deep roots to extract water are not known.

83 Improving our understanding of soil water provisioning of forests is particularly relevant in  
84 the context of climate change, because terrestrial ecosystems are facing an increase in atmospheric  
85 evaporative demand (Grossiord et al., 2020) and projections of reduced summer precipitation point

86 to a likely increase in edaphic water stress over the coming decades in most continents and notably  
87 Western Central Europe and the Mediterranean zone (Samaniego et al., 2018). How forests react  
88 to increased water deficit will depend, to a large extent, on their access to soil water.

89 Recent summer drought and heat events observed over large parts of Europe (year 2003 in  
90 Western Europe, 2010 in Russia, 2018 in Northern central Europe; Bastos et al., 2020) have  
91 constituted natural experiments documenting the influence of warmer and drier conditions on  
92 ecosystem carbon and water fluxes. In particular, the combined summer 2003 drought and heat  
93 caused a seasonal reduction of gross and net carbon uptake (Reichstein et al., 2007; Bastos et al.,  
94 2020), as well as of evapotranspiration, in response to soil water stress (Granier et al., 2007).

95 As the return period of combined drought and heat events decreases with ongoing climate  
96 change (Samaniego et al., 2018), it is urgent to improve our understanding of the provisioning of  
97 water to forest ecosystems, and to evaluate the sensitivity of modelled projections of ecosystem  
98 functioning to the parameterization of soil properties.

99 Here we used soil water content data measured over a 150-cm soil profile, combined with deep  
100 soil water content estimates (i.e. sensors down to -300 cm) to evaluate the role of surface vs. deep  
101 water in provisioning tree transpiration needs and modulating canopy gas exchange in a temperate  
102 oak forest. We focused on the two contrasted, consecutive years of 2017 (a mild summer) and 2018  
103 (characterized by a hot drought). Our objectives were:

- 104 1. to evaluate the response of a temperate oak forest to a hot drought in terms of carbon and  
105 water balances,
- 106 2. to estimate the Soil Water Holding Capacity (SWHC, in millimeters of water) of the forest,
- 107 3. to estimate the contribution of soil horizons to the provision of water for canopy transpiration,  
108 contrasting both a dry and milder year,
- 109 4. to evaluate how the combinations of SWC and VPD modulate canopy conductance and  
110 transpiration,
- 111 5. to compare two estimates of SWHC: one provided by soil databases vs. one derived from  
112 our measurements of SWC, and quantify the sensitivity of the carbon balance simulated by

113 a process-based model to the choice of one or the other SWHC estimate.

## 114 **Materials and Methods**

### 115 **Study site**

116 The Fontainebleau-Barbeau site (FR-Fon, Delpierre et al., 2016) is located in the Paris area,  
117 near the Fontainebleau forest (48.476358 N, 2.780120 E, 103 m a.s.l.). The site has a gentle slope  
118 of 2° towards the Seine river which flows 750 m at the South-West of the flux tower. Sessile oak  
119 (*Quercus petraea* (Matt.) Liebl.) is the main species, accounting for 79% of the basal area and  
120 dominating an understorey mostly occupied by hornbeam (*Carpinus betulus* L., 18% of the basal  
121 area). The dominant height is 28 m. The soil is an endostagnic luvisol (IUSS Working Group  
122 WRB, 2015) covered by an oligo-mull humus. It developed on a calcareous bedrock located at  
123 5-10 m-depth (Thiry, 2010) and has a discontinuous buhrstone layer located between 60 to 90-cm  
124 depth, over which a perched water table develops in winter, usually till late spring. Mean annual  
125 air temperature and cumulated precipitation are 11.2°C and 677 mm, respectively (1980–2010,  
126 Melun weather station, 12 km from the study site). The leaf area index (LAI) was on average  
127 6.01 over the 2012–2018 period. In spring 2021, we established the root distribution at FR-Fon by  
128 counting roots according to diameter class in a 2-m wide and 150-cm deep trench dug 50 meters  
129 away from the flux tower. We noticed the presence of fine roots down to the bottom of the trench  
130 (-150 cm; Suppl. Mat. S1). In autumn 2021, we extracted one 5-m deep core sample, also in the  
131 vicinity of the flux tower. On this unique sample of 10-cm diameter, we observed the presence of  
132 1-mm diameter roots down to a depth of 4 meters (Suppl. Mat. S1), at the top of a dense green  
133 marl layer.

### 134 **Eddy covariance and micrometeorological measurements.**

135 We measured the fluxes of CO<sub>2</sub> and H<sub>2</sub>O between the forest and the atmosphere with the eddy  
136 covariance (EC) method, using both a Li7500 open-path and a Li7200 enclosed-path analyzer  
137 (LI-COR Inc., Lincoln, NE, USA), associated with a R3-50 and a HS-50 sonic anemometer (Gill

138 Instruments Ltd., Lymington, UK), respectively. Both EC systems runned concurrently at 37  
139 m a.g.l., i.e. 9 m above the dominant height. EC data were acquired at 20 Hz with two data  
140 loggers time-synchronized with a PTP server: a CR3000 (Campbell Scientific Inc., Loughborough,  
141 UK) for the Li7500/R3-50 and the Smartflux 2 for the Li7200/HS-50 (LI-COR Inc., Lincoln, NE,  
142 USA). Half-hourly fluxes of CO<sub>2</sub> and H<sub>2</sub>O were calculated using the EddyPro software (v7.0.6,  
143 LI-COR Inc., Lincoln, NE, USA). Frequency response corrections were applied to raw fluxes,  
144 accounting for high-pass (Moncrieff et al., 2005) and low-pass filtering (Moncrieff et al., 1997).  
145 The influence of air density fluctuations on the fluxes was accounted for (Burba et al., 2008).  
146 As usually done (Baldocchi, 2008), we did not correct eddy covariance fluxes despite a  $18\pm 6\%$   
147 average energy imbalance (calculated as the Energy Balance Ratio, Wilson et al., 2002) at the  
148 FR-Fon site. Half-hourly CO<sub>2</sub> and H<sub>2</sub>O fluxes have been acquired continuously from 2005 by the  
149 Li7500/R3-50 device and were considered the reference data series here. Fluxes computed from  
150 the Li7200/HS-50 device, running from 2012, were used to gap-fill the reference data through  
151 linear regressions established annually. Following this instrumental gap-filling, the calculated Net  
152 Ecosystem Productivity (NEP) and evapotranspiration (ETR) fluxes were quality-controlled, gap-  
153 filled, and NEP was partitioned into Gross Primary Productivity (GPP) and ecosystem respiration  
154 (Reco) according to standard procedures (Reichstein et al., 2005; Papale et al., 2006). We estimated  
155 the uncertainty of annual GPP and NEP values as the combination of uncertainties originating from  
156 the choice of a  $u^*$  threshold for filtering the data, and the propagation of random error inherent  
157 to EC measurements during the statistical inference by the gap-filling algorithms (Delpierre et al.,  
158 2012). ETR is an integrative measurement of the quantity of water evaporated from both wet  
159 surfaces (soil and canopy) and plant transpiration. Here we partitioned the eddy-covariance ETR  
160 flux into (i) the canopy plus topsoil litter evaporation flux, that do not affect the amount of water  
161 held in the organo-mineral horizons of the soil and (ii) the transpiration plus soil evaporation  
162 flux (TrSeF), that tap the soil water stock. For doing so, we applied to eddy-covariance ETR  
163 data the ratio of TrSeF to ETR calculated hourly by the CASTANEA model (see e.g. Nelson  
164 et al., 2018). Air temperature and relative humidity used to calculate the vapor pressure deficit  
165 (VPD) were measured at 37 m a.g.l with a HMP155A thermohygrometer (Vaisala Corp., Helsinki,

166 Finland) protected from radiation with a 43502H aspiration radiation shield (R. M. Young, Traverse  
167 City, MI, USA). Precipitation was measured with a ARG100 raingauge (EML, North Shields, UK  
168 raingauge) located at 36 m a.g.l.

## 169 **Soil water content**

170 **Data acquisition.** Soil water content (SWC, in  $\text{m}^3_{\text{water}} \text{m}^{-3}_{\text{soil}}$ ) was measured from 2012 with five  
171 EnviroSCAN probes (Sentek Sensor Technologies, Stepney, Australia) located in the vicinity of  
172 the tower and connected to a CR1000 datalogger. Each probe had a 10-cm vertical distribution of  
173 15 sensors from -5 cm to -145 cm, i.e. down to 150 cm depth. From 2016, a sixth probe reached  
174 the depth of -300 cm with the following vertical sensor distribution: -15, -55, -85, -135, -175, -215,  
175 -255, and -295 cm. The CR1000 datalogger achieved automatic data acquisition with half-hourly  
176 means calculation. In order to assess the spatial representativity of SWC measurement collected  
177 by the 6 probes, 24 access tubes of 160 cm long were installed in the vicinity of the tower in 2012  
178 over a 3800-m<sup>2</sup> area. We measured SWC in those tubes on a weekly basis, with a DIVINER probe  
179 (Sentek Sensor Technologies, Stepney, Australia), measuring SWC in the soil profile at multiple  
180 depths (at 10 cm intervals), comparable to the profiles obtained with the EnviroSCAN probes.  
181 The EnviroSCAN and DIVINER measurements are based on high-frequency capacitance. Since  
182 no soil-specific calibration of the probes was achieved on the Fontainebleau-Barbeau site, SWC  
183 were calculated from the scaled frequency of the probes using the factory calibration equation. We  
184 tested the sensitivity of the calibration equation, following the work of Provenzano et al. (2016),  
185 and found minor influence on the SWC dynamics, in accordance with observations by the probe  
186 manufacturer (Sentek Pty Ltd, 2001).

187 **Estimation of the Soil Water Holding Capacity.** We estimated the integrated SWHC down  
188 to 300 cm using the following equation:

$$SWHC = \sum_{i=1}^{30} (FC_i - PWP_i) \delta h \quad (1)$$

189 with the index  $i$  identifying soil layers of  $\delta h = 10$  cm depth down to 300 cm. We identified FC

190 (Field Capacity, i.e. the maximum moisture of unsaturated soil, in  $\text{m}^3_{\text{water}} \text{m}^{-3}_{\text{soil}}$ ) for each soil layer,  
 191 by looking at periods of stable, relaxed SWC following soil saturation occurring typically occurring  
 192 in early spring. For each soil layer, we identified the permanent wilting point (PWP, in  $\text{m}^3_{\text{water}}$   
 193  $\text{m}^{-3}_{\text{soil}}$ ) as the lowest SWC value for that soil layer, typically reached during dry summer periods.  
 194 As SWC drops to PWP, root water uptake, and the associated daily oscillations of SWC, tend to  
 195 zero in the considered soil layer. We illustrate the basic procedure to extract FC and PWP for the  
 196 layer between 120 and 130 cm (index  $i=13$ ) in Fig.2, assuming the PWP is reached in the very dry  
 197 year 2018. For each layer in the 0-160 cm zone, FC and PWP have then been deduced from the  
 198 SWC closest sensors. The highest vertical resolution (equal to 10 cm) and representativeness of  
 199 the spatial variability (20 probes) is obtained for indexes  $i= 1$  to 16 (i.e. 10 to 160 cm depth). Less  
 200 information was available for the deeper layers (160-300 cm). In that case, a unique automatic  
 201 probe measuring SWC at 180, 220, 260, and 300 cm has been used to investigate soil layers  $i= 17$   
 202 to 30. As a consequence, and because we suspected those deep soil layers to remain above PWP  
 203 in year 2018 (see below), we used FC and PWP determined over  $i=14$  to 16 as representative of  
 204 soil layers  $i= 17$  to 30 (Suppl. Mat. 4).

205 **Estimation of SWHC uncertainty.** We assumed the SWHC uncertainty to result from the  
 206 reading of PWP and FC on the SWC time series and the spatial (among-probes) variability. The  
 207 reading uncertainty was estimated at  $\sigma_r= 1$  mm for PWP and FC respectively. The uncertainty  
 208  $\sigma_{s,i}$  attributed to spatial variability can be accurately estimated for each 10-cm layer  $i$  thanks to  
 209 the DIVINER probe exploring a 3800- $\text{m}^2$  area over 160 cm (see above). For deeper (170-300 cm)  
 210 layers, we hypothesized  $\sigma_{s,i}$  was equal to the average value in the upper zone. As a consequence,  
 211 we calculated the the overall SWHC uncertainty as:

$$\sigma = \sqrt{\sum_{i=1}^{30} (\sigma_{s,i}^2 + 2\sigma_r^2)} \quad (2)$$

212 where  $i$  index denotes the layer number ranging from 1 (layer 0-10 cm) to  $N=30$  (layer 290-300  
 213 cm).

## 214 **Calculation of Root Water Uptake.**

215 The amount of water uptaken from the soil by trees, the so-called RWU flux (Root Water  
216 Uptake, in  $\text{mm day}^{-1}$ ), can be calculated from SWC time series (Hupet et al., 2002). The major  
217 interest of using SWC data to infer RWU is that it does not require any prior knowledge of the  
218 root distribution. In that context, different methods exist to extract RWU, from numerical model  
219 inversion (Zuo and Zhang, 2002) to the use of daily fluctuations in SWC (Li et al., 2002). Indeed,  
220 RWU manifests as fluctuations in soil moisture in the rhizosphere, influenced by evapotranspiration  
221 which occurs preferentially over daytime. As a consequence, RWU can be assessed using linear  
222 regression and differentiation of daytime vs. nighttime change in SWC. In a methods comparison  
223 (Guderle and Hildebrandt, 2015), this approach using daily SWC oscillations proved to be the  
224 best regarding a combination of criteria: the quality of estimations and lesser induced error due to  
225 moisture sensor accuracy (the calibration error). Consequently, we focused on this method, and  
226 calculated RWU at our site from SWC measurements with the python package *rootwater* (Jackisch  
227 and Mälicke, 2020). This algorithm analyses daily fluctuations in SWC and takes into account  
228 possible hydraulic redistribution, a mechanism by which water is moved via the root system from  
229 moister to drier soil layers (Caldwell et al., 1998; Ishikawa and Bledsoe, 2000; Neumann and Cardon,  
230 2012). We applied the *rootwater* algorithm on days when SWC profiles exhibited the specific  
231 transpiration-induced shape of RWU (i.e. daytime decline of SWC). We therefore rejected days  
232 displaying strong drainage along the soil profile, which could blur the effect of RWU. For selected  
233 days, a reference daily moisture profile was built, based on the SWC values at sunset/sunrise, and  
234 linear interpolations. The reference reflects “perfect” RWU over daytime and diffusion over night  
235 time (Jackisch et al., 2020). The theoretical step shape profile was then compared to the observed  
236 profile thanks to an evaluation of the Nash–Sutcliffe efficiency (NSE, Nash and Sutcliffe, 1970).

## 237 **Response of canopy conductance to VPD and SWHC.**

238 In order to evaluate how the combinations of SWC and VPD modulated canopy conductance  
239 ( $G_{can}$ ) and evaporation, we first calculated  $G_{can}$  through inverting the Penman-Monteith equation,  
240 as in Novick et al. (2016). We then fitted  $G_{can}$  as a function of VPD with the following equation

241 (Novick et al., 2016):

$$G_{can} = G_{can,ref}[1 - m \times \ln(VPD)] \quad (3)$$

242 where  $G_{can}$  is the canopy conductance for water vapor ( $\text{mmol m}^{-2} \text{s}^{-1}$ ),  $G_{can,ref}$  is its value at  
243 reference VPD of 1 kPa, and  $m$  ( $\ln(\text{kPa})^{-1}$ ) is the slope of the relation. We fitted this equation  
244 for different classes of soil humidity, computed as Relative Extractable Water (REW, defined as  
245  $\text{REW} = \text{SWC}_{0-300\text{cm}}/\text{SWHC}_{0-300\text{cm}}$  where  $\text{SWC}_{0-300\text{cm}}$  is the actual stock of water extractable by  
246 trees, in millimeters, over a 300-cm soil depth for a given day and  $\text{SWHC}_{0-300\text{cm}}$  is the maximum  
247 water content extractable by trees, in millimeters, over a 300-cm soil depth).

## 248 **CASTANEA model**

249 One of our objectives was to determine the sensitivity of ecosystem models to parameterizations  
250 of SWHC. To this aim, we used the CASTANEA model (Dufrêne et al., 2005) to simulate  $\text{CO}_2$   
251 (namely GPP) and  $\text{H}_2\text{O}$  (namely ETR) fluxes at FR-Fon, under different climate conditions.  
252 CASTANEA is a process-based ecosystem model that simulates the forest carbon and water fluxes  
253 (including transpiration, canopy, litter and soil evaporation) at an half-hourly time step. First, we  
254 calibrated some of the model most sensitive parameters (Supplementary notes SN1) in order to  
255 simulate GPP and ETR accurately over periods with no water stress over the period of 2006-2019.  
256 Then, we performed prospective simulations under a changing climate, considering three climate  
257 models under two RCP scenarios (RCP4.5 and 8.5, see Jourdan et al., 2021 for details on the  
258 climate models). With those simulations, we quantified the sensitivity of simulated GPP to the  
259 SWHC parameter. SWHC is a forcing parameter to the model, and has been identified as very  
260 sensitive, with 10% variation of SWHC yielding 13-24% variations of annual NEP, 5-8% variations  
261 of annual GPP and 3-4% variations of annual ETR in simulated fluxes (Dufrêne et al., 2005).

## 262 **Soil database for parameterizing SWHC.**

263 We parameterized CASTANEA with two different SWHC estimates at the FR-Fon forest. We  
264 used our own estimate of SWHC, based on SWC measurements (see Results). Beside this, and  
265 similar to what is usually done for parameterizing ecosystem models (e.g. Cheaib et al., 2012), we  
266 used a SWHC estimate obtained from a soil database (Badeau et al., 2010). Badeau et al. built a  
267 1-km<sup>2</sup> resolution database of SWHC over France, from a soil database of soil texture and rooting  
268 depth (Jamagne et al., 1995). Each 1x1 km grid point encompasses different soil types, and the  
269 database gives for each grid point the average value of SWHC with respect to the area of each soil  
270 type over the 1x1 km grid.

## 271 Results

### 272 Annual fluxes and climatic water balance

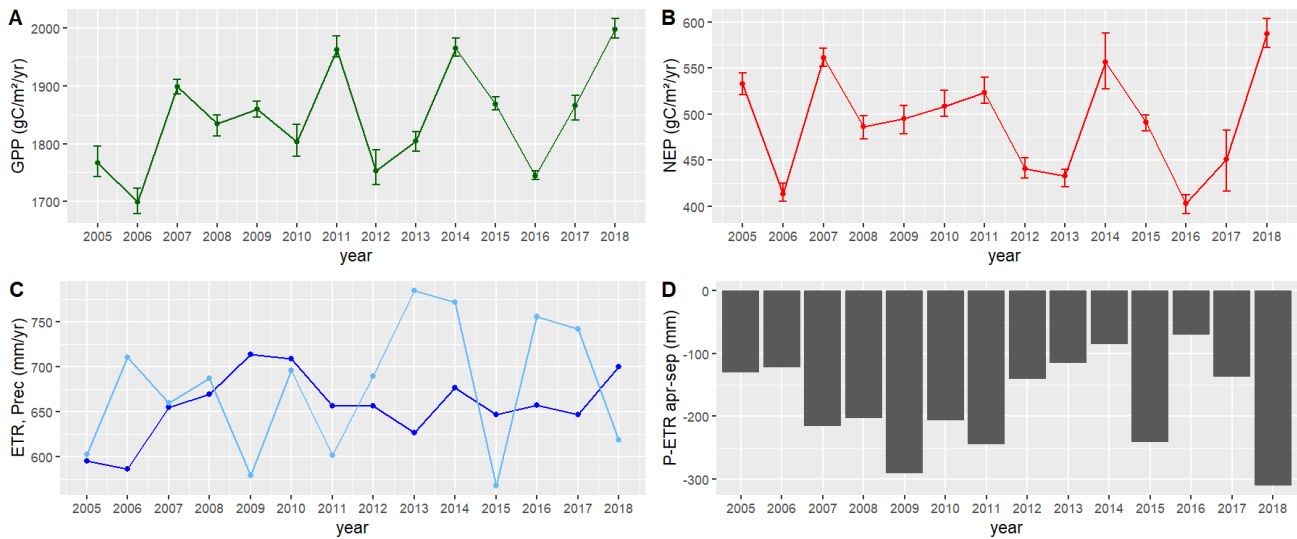


Fig. 1: Annual carbon and water fluxes at FR-Fon for the period 2005-2018. (A) displays the annual gross primary productivity (GPP), (B) the net ecosystem productivity (NEP), (C) the annual precipitation (Prec, light blue) and evapotranspiration (ETR, dark blue) and (D) a climatic water balance, namely the difference between Apr-Sep precipitation and evapotranspiration. In (A) and (B), error bars display the 5th and 95th percentile of the GPP and NEP uncertainty distributions (see text for details).

273 The growing season (April-September) climatic water balance (P-ETR) was largely negative  
274 on all years (-179 mm on average) and reached its lowest value in 2018 (-310 mm; Fig.1d). In spite  
275 of this, year 2018 was the year of highest GPP ( $1997 \text{ gC m}^{-2} \text{ y}^{-1}$ , Fig.1a) and the year of highest  
276 NEP on record ( $587 \text{ gC m}^{-2} \text{ y}^{-1}$ , Fig.1b), as compared to averages of  $1844 \text{ gC m}^{-2} \text{ y}^{-1}$  and  $491$   
277  $\text{gC m}^{-2} \text{ y}^{-1}$  respectively over 2005-2018. Annual evapotranspiration averaged  $657 \text{ mm y}^{-1}$  over  
278 2005-2018, and reached its third highest value in 2018 ( $700 \text{ mm y}^{-1}$ , Fig.1c). Accordingly, when  
279 considering seasonal patterns, GPP, NEP and ETR appeared not influenced by the climatic water  
280 deficit evolving over the 2018 growing season (Suppl. Mat. S3 and S5).

### 281 Estimation of SWHC

282 In order to estimate SWHC, we focused on year 2018, which was the driest on record (based  
283 on the climatic water balance data, Fig. 1d; see also the comparison of 2017-2018 soil water  
284 content data, Suppl. Mat. S5). In that year, we observed seasonal variations of soil water content

285 down to 300 cm, which was the location of the deepest SWC probe. In the 290-300 cm layer,  
286 SWC fluctuated from 0.31 to 0.25 m<sup>3</sup>/m<sup>3</sup> during year 2018, reaching its maximum in July and its  
287 minimum in November (Fig.2a). The seasonal dynamics at 290-300 cm was clear, although less  
288 ample than at a shallower layer (e.g. 120-130 cm, Fig.2a) where it fluctuated from 0.36 (end of  
289 June) down to 0.23 m<sup>3</sup>/m<sup>3</sup> (November, Fig.2a). Interestingly, we observed daily fluctuations of  
290 the SWC signals at all measurements depths, down to 290-300 cm (Fig.2b). The daily fluctuations  
291 were neat from May at 120-130 cm depth and their amplitude increased in July, when they also  
292 became visible in the 290-300 cm layer (Fig.2b). As for the upper layers (not shown), the SWC  
293 signal had a clear shape in the 290-300 cm layer, with a decrease during the day and a stall during  
294 the night, which was evocative of the day/night cycle of tree transpiration, and root water uptake  
295 (Fig.2a inset).

296 We estimated the quantity of water extractable in each soil layer from SWC measurements  
297 (Suppl. Mat. S4). Field capacity (FC, the maximum moisture of unsaturated soil) was consid-  
298 ered to be reached when SWC reached stable, high values (e.g. skyblue dashed line on Fig.2a),  
299 after checking the disappearance of a seasonal perched water table from piezometer data (not  
300 shown). We supposed that one soil layer had reached the permanent wilting point (PWP) when  
301 SWC reached a stable, low value (e.g. red dashed line on Fig.2a). We only had one probe for  
302 characterizing the water availability deeper than 160 cm (measuring at depths 170-180, 210-220,  
303 250-260 and 290-300 cm, cf. Material and Methods), as opposed to 20 probes for shallower layers  
304 (0-160 cm). Below 160 cm, it was also difficult to identify clear FC and PWP values (e.g. for the  
305 290-300 cm layer on Fig.2a). Hence we extrapolated values of FC and PWP obtained for the layers  
306 140-160 cm (Suppl. Mat. S4) to deeper layers, which is coherent with the homogeneous nature  
307 of the soil (sandy loam) over 120-300 cm. We calculated SWHC to reach 390 mm over 0-300 cm,  
308 with an estimated uncertainty of 17 mm, combining the reading uncertainty of FC and PWP, and  
309 the variability observed among the 20 measurements probes.

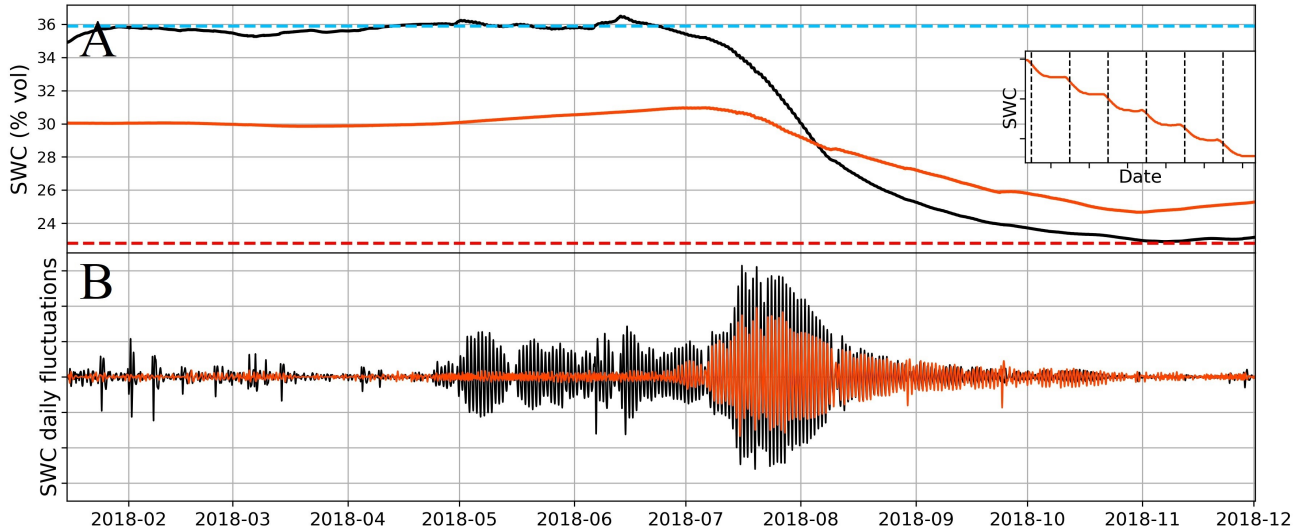


Fig. 2: SWC time series of the layer 120-130 cm (black color) and 290-300 cm (orange color) during the 2018 dry year. (A) displays the measured SWC profile calculated as the mean of five 160-cm length EnviroSCAN probes (for layer 120-130 cm); one 300-cm length EnviroSCAN probe (for layer 290-300 cm). The skyblue- and red-dashed lines are the FC and PWP values for layer 120-130 cm, respectively. (B) displays results from a passband filter (fourth-order Butterworth filter) applied to the SWC profiles and centered around daily fluctuations. The inset in (A) is a zoom on SWC profile at 290-300 cm between 2018-08-02 and 2018-08-08, with vertical dashed lines indicating midday.

## 310 Seasonal and interannual patterns of root water uptake

311 The root water uptake (RWU) flux calculated from the *rootwater* algorithm applied over 0-300  
 312 cm compared generally well with the transpiration fluxes derived from ET measurements (Fig.3).  
 313 Both the seasonal shapes, and the actual flux values were similar between those independent  
 314 methods. The *rootwater* algorithm tended to generate lower flux values as compared to the ET-  
 315 derived transpiration (average of 2.22 vs. 2.34 mm/day, respectively, in 2017 and 2.34 vs. 2.56  
 316 mm/day in 2018) though the extrema were similar (minima of 0 and maxima of 6-7 mm per  
 317 day). From Figure 3 we inferred that water extraction could occur deeper than 300 cm since  
 318 RWU (calculated over 0-300 cm) was generally lower than the ET-derived transpiration flux and  
 319 appeared noticeably underestimated in year 2018 on DoY 240- 260, when extraction from deep  
 320 horizons was particularly strong (see below).

321 The seasonal patterns of RWU in individual soil layers are displayed on Fig.4. The contribution  
 322 of deep layers increased as superficial layers dried up. The plasticity of RWU was fast. For instance,  
 323 the contribution of the 0-150 cm layers decreased from 72% to 55% over 12 days (DoY 165 to 176  
 324 in 2017, Fig.4a); from 69% to 51% over 7 days (DoY 214 to 220 in 2017, Fig.4a); and from 64%

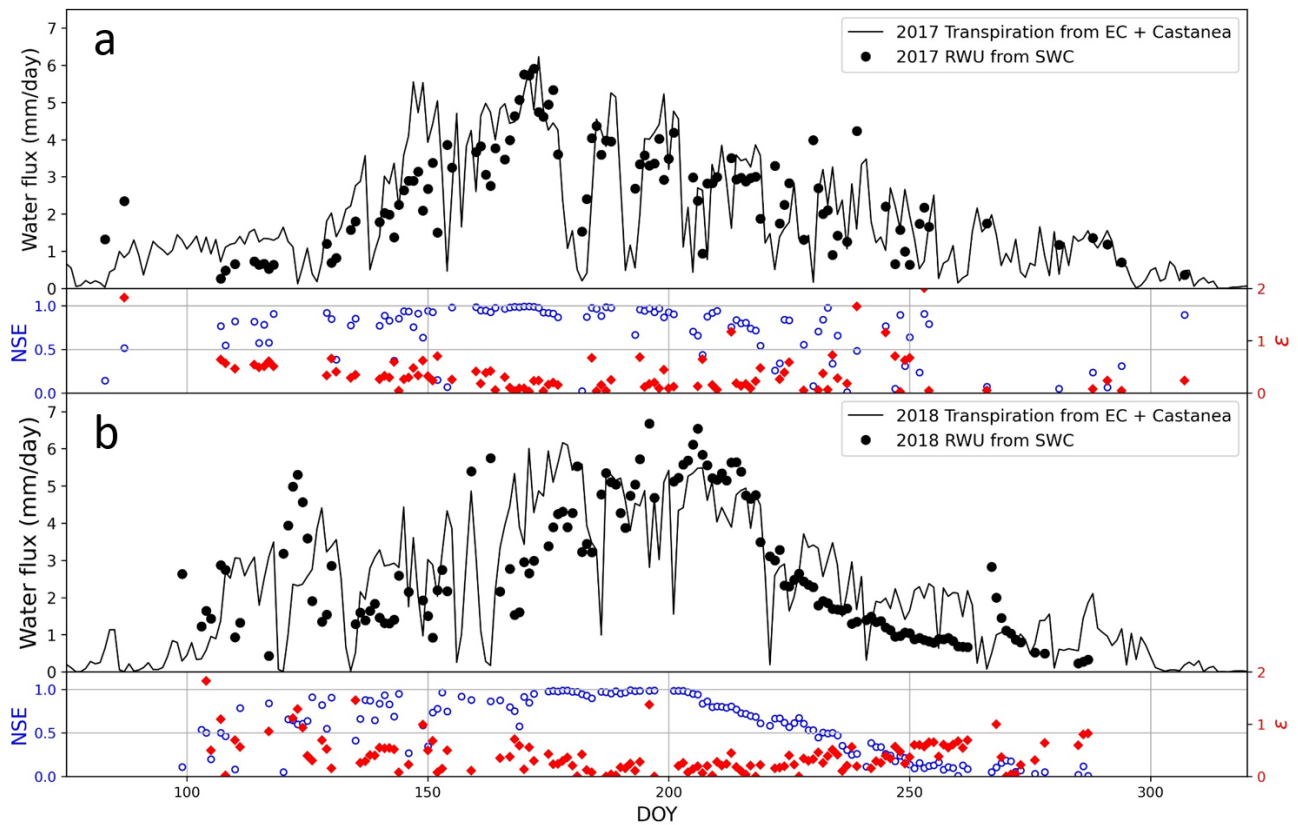


Fig. 3: Daily water fluxes in mm per day over the year in 2017 (a) and 2018 (b). Black dots illustrate the root water uptake (RWU) calculated from the soil water content (SWC) integrated over 300 cm, assuming no hydraulic redistribution. The black-solid line corresponds to tree transpiration (T) resulting from the daily average evapotranspiration fluxes calculated from the flux tower (EC), from which T was deduced thanks to the CASTANEA ecosystem model (see text). Red markers represent the absolute relative error between the water fluxes estimated from SWC and EC which is obtained as  $\varepsilon = \text{abs}(\text{RWU}-T)/T$ . Blue dots represent the daily NSE values of the *rootwater* algorithm applied over 0-300 cm.

325 to 43% over 21 days (DoY 198 to 217 in 2018, Fig.4b). More generally, the role of deep water  
 326 extraction increased over the growing season. Before DoY 160, the contribution to RWU of layers  
 327 deeper than 150 cm was less than 20% in both years. This contribution went up to more than 40%  
 328 and almost 60% on DoY 220, for 2017 and 2018 respectively.

329 RWU seasonal patterns differed for years 2017 and 2018, owing to their meteorological char-  
 330 acteristics. For instance, over the period of DoY 160-180, we observed deeper water extraction in  
 331 2017 as compared to 2018, in relation with drier soil conditions (Suppl. Mat. S5). In the same  
 332 logic, the drier period of DoY 220-260 in 2018 showed a deeper water extraction as compared to  
 333 2017.

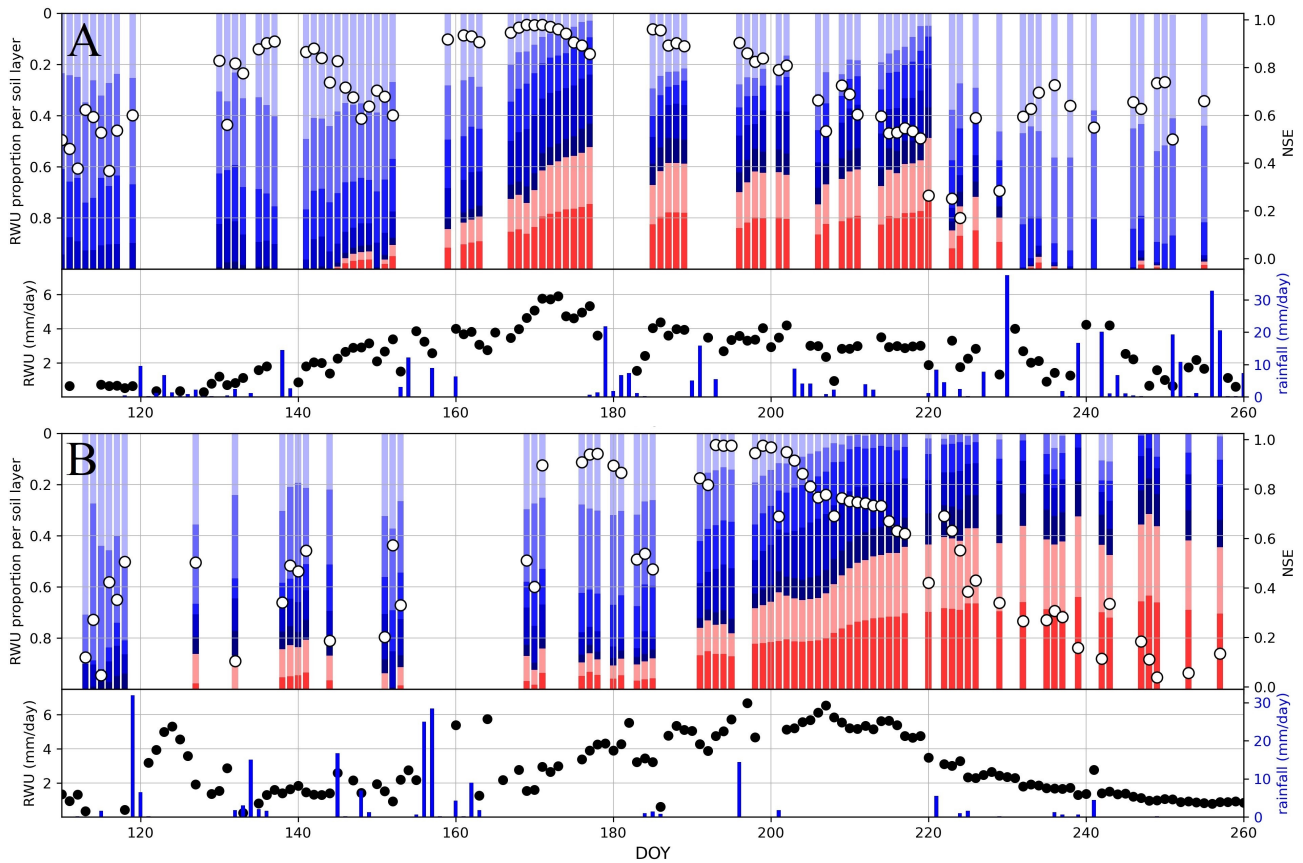


Fig. 4: Root water uptake (RWU) dynamics in 2017 (a) and 2018 (a). The RWU in  $\text{mm day}^{-1}$  was estimated using the *rootwater* algorithm on the integrated soil water content considered over 0-300 cm depth. The proportion per horizon was obtained using the information on separated layers, assuming hydraulic redistribution if observed on the SWC profile. The colors corresponded to different layers, from lightest to darkest blue: 0-30 cm, 30-60 cm, 60-90 cm, 90-120 cm and 120-150 cm depth. Layers 150-220 cm and 220-300 cm are in light red and dark red respectively. Five EnviroSCAN probes were used to calculate RWU over 0-150 cm, one probe was used over 150-300 cm (see text). White dots (right axis) represent NSE values of the *rootwater* algorithm. Blanks in the RWU time series mark episodes of high precipitation (typically above 5 mm per day) hindering the estimation of RWU by the algorithm.

### 334 Soil influences canopy conductance despite high SWHC.

335 The contribution of deeper layers to RWU increased as soil dryness developed over the growing  
 336 season. This revealed the plasticity of water uptake to maintain high levels of evapotranspiration.  
 337 Yet this plasticity was limited by the total amount of water in the soil, as shown in Fig.5. On  
 338 panels (a) and (b), half-hourly latent heat fluxes were plotted against the Relative Extractable  
 339 Water (REW) defined as  $\text{REW} = \text{SWC}/\text{SWHC}_{0-300\text{cm}}$ , over the period DoY 165-255. REW  
 340 decreased from 0.6 to 0.2 in 2017 (Fig.5a) and from 1.0 (i.e. field capacity) to 0.1 in 2018 (Fig.5b).  
 341 The large REW range explored over 2018 made the correlation between latent heat fluxes and  
 342 REW clearly visible (Fig.5b). Latent heat fluxes showed no trend along REW for high REW

343 values (typically over 0.6) and decreased as REW decreased.

344 Figure 5c further illustrated the dual control exerted by REW and VPD on canopy conductance.  
345 Canopy conductance decreased with both VPD and REW (Fig.5c). At a reference VPD of 1 kPa,  
346 canopy conductance ( $G_{can}=G_{can,ref}$ ) decreased from 0.52 to 0.32 mol m<sup>-2</sup> s<sup>-1</sup> (Fig.5c) as REW  
347 decreased from 0.87 to 0.12 (Fig.5e, showing that the values are comparable to those reported by  
348 Novick et al., 2016 for mesic sites), while  $m$ , the slope of the relation between,  $G_{can}$  and VPD,  
349 was in the range [0.46; 0.66], apparently increasing as REW decreased (Fig.5d, also showing data  
350 in line with Novick et al., 2016), noting that the comparison of the  $m$  slopes along REW may be  
351 uncertain because  $m$  at low soil water content was estimated from a fit established over a narrow  
352 VPD range (red curve on Fig.5c) .

### 353 **Sensitivity of an ecosystem model to SWHC parameterization.**

354 The SWHC value of 390 mm determined from SWC measurements was 1.9 times higher than  
355 the value of 207 mm estimated from the 1-km French soil database for the corresponding grid  
356 point (Badeau et al., 2010), and in the high end of the SWHC distribution of soils appearing  
357 in the database over France (Fig.6a). The CASTANEA model fairly simulated the seasonality  
358 of GPP observed at FR-Fon when parameterized with SWHC= 390 mm (Fig.6b), as well as the  
359 interannual variability of GPP (Suppl. Mat. SN1). On the contrary, parameterizing CASTANEA  
360 with SWHC= 207 mm, as obtained from the soil database (Badeau et al., 2010) led to higher  
361 soil water stress and reduced GPP in summer, as compared to GPP derived from the flux tower  
362 measurements (Fig.6b). Over the period 2006-2019, annual GPP simulated with SWHC= 390  
363 mm were 365 gC m<sup>2</sup> y<sup>-1</sup> higher than with SWHC= 207 mm. The GPP anomaly caused by the  
364 under-estimation of SWHC in the model parameterization remained rather stable in future climate  
365 conditions under RCP4.5 scenario, but nearly doubled to 700 gC m<sup>2</sup> y<sup>-1</sup> for two out of three climate  
366 models under RCP8.5 (Fig.6c).

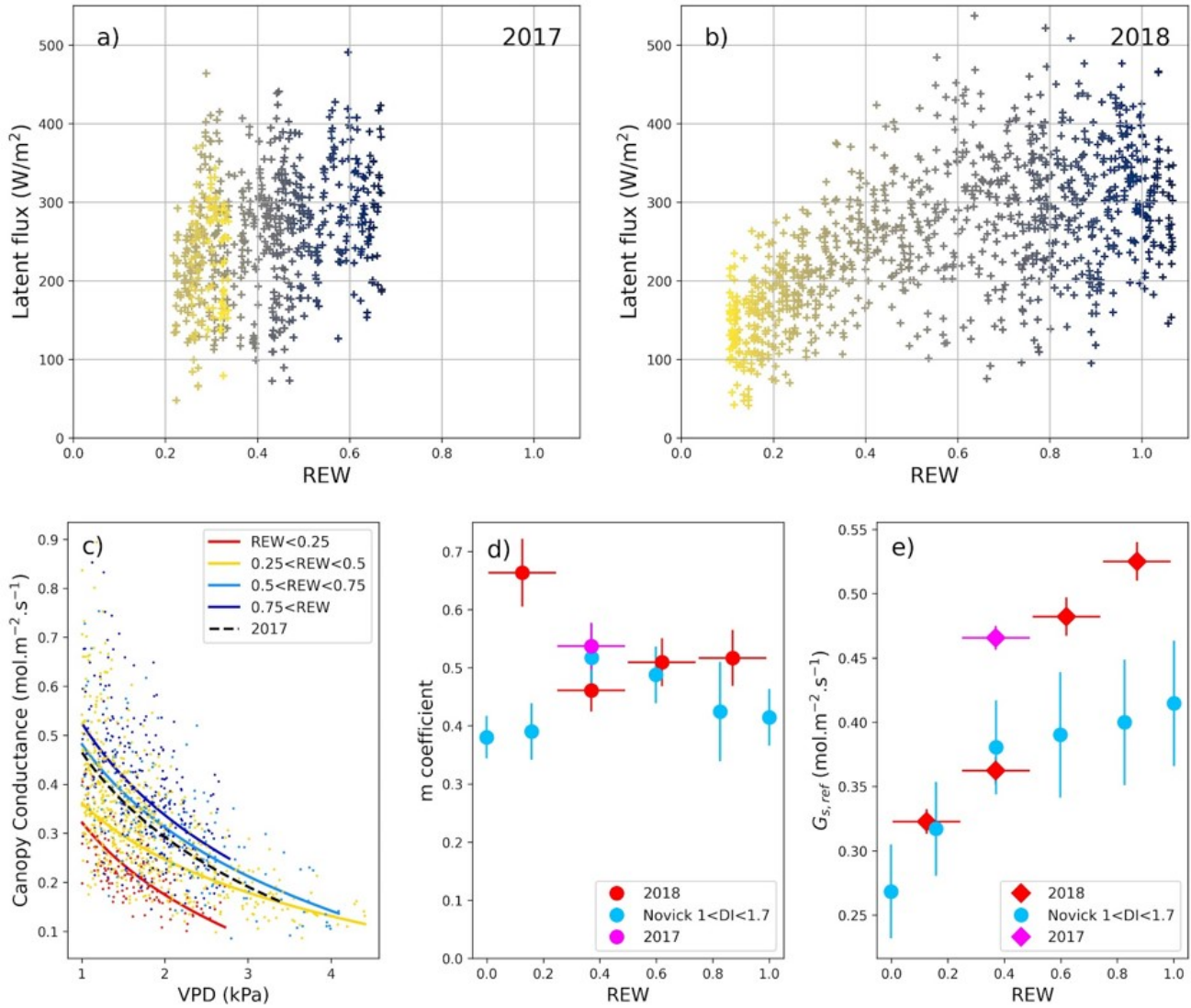


Fig. 5: Effect of SWC and VPD on canopy conductance and evapotranspiration. The data plotted were selected in  $165 < \text{DoY} < 255$ , between 10 am and 6 pm, with  $\text{VPD} \geq 1$  kPa and latent heat flux  $\geq 150$   $\text{W/m}^2$ . In (a) and (b), the point colors refer to DoY, with the darkest points for DoY 165 and the yellowest points for DoY 255. In (c), the lines represent the fit of equation 3 for different intervals of REW, with the colored lines being for 2018 while the black dashed line is for 2017 with  $0.25 < \text{REW} < 0.5$ . Panels d) and e) display the values of  $m$  and  $G_{s,ref}$  calculated from our data as well as those calculated by Novick et al. (2016) (their Figure 2 e and f) over an ensemble of Ameriflux sites. We represented here average values obtained at sites comparable to Fontainebleau-Barbeau according to values of the Dryness Index (the ratio of annual PET to annual P, with values from 1.0 to 1.7). For the sake of comparison, SWC data reported by Novick et al. (2016) (over 0-30 cm) were converted to REW by dividing the actual SWC value by the maximum SWC value reported on their figure.

## 367 Discussion

368 **Influence of Drought 2018 on carbon and water fluxes at FR-Fon.** The growing season  
 369 of 2018 was amongst the driest encountered at FR-Fon over the past 40 years (ranked sixth over  
 370 the period 1980-2018 as regards the difference of P-PET, not shown). Yet the annual produc-

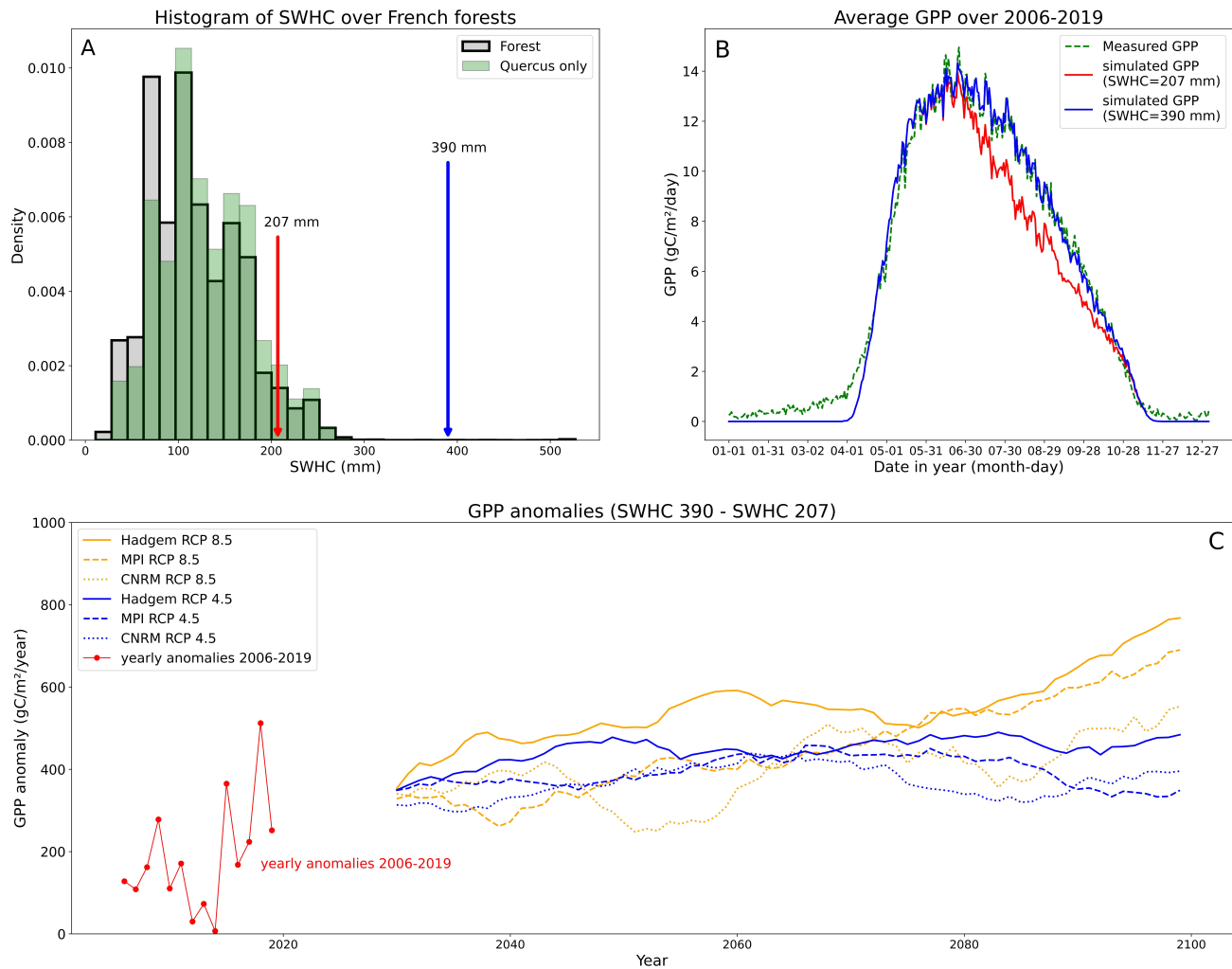


Fig. 6: Sensitivity of the CASTANEA model simulations to the parameterization of Soil Water Holding Capacity (SWHC). (a) Distribution of the SWHC values in the French Soil Database, with all 1-km<sup>2</sup> pixels occupied by forests (grey bars, n= 68 373 points) and forest pixels mostly occupied by deciduous oaks (n= 35 352 points). Red arrow point to the SWHC estimate obtained for FR-Fon grid point in the Badeau et al. (2010) database, Blue arrow point to our estimate of SWHC, obtained from the analysis of SWC measurements; (b) Comparison of GPP calculated from the FR-Fon flux tower measurements with CASTANEA simulations for two values of SWHC (390 mm and 207 mm), averaged over the 2006-2019 period; (c) Projections of simulated difference in GPP between CASTANEA model runs using SWHC= 390 mm and SWHC= 207 mm over the 2020-2100 period (lines displayed are the 20 years rolling averages). Three climatic models were considered (Hadgem, MPI and CNRM) with two CO<sub>2</sub> emission scenarios for each (RCP 4.5 and RCP 8.5). The red points at the beginning of the time series illustrate the average anomaly calculated over 2006-2019.

371 tivity remained high, with the highest annual NEP and highest annual GPP from the start of  
 372 flux measurements in 2005 (Fig.1a,b). Lower than average GPP values over July-October were  
 373 compensated by higher than average GPP over April-July (Suppl. Mat. S3b), probably owing to  
 374 higher than average temperatures and radiation (Suppl. Mat. S2a,b). The higher than average  
 375 spring photosynthesis was not caused by an early budburst, which occurred on DoY 105 for oaks  
 376 (i.e. equal to the average 2006-2018 date, Soudani et al., 2021). The July-October 2018 negative

377 anomaly of GPP was moderate, probably in relation to the high SWHC. Indeed, a lower SWHC  
378 would have resulted in lower GPP (Fig.6b). Higher than average NEP were encountered during  
379 most of the growing season, and notably during July-October, when GPP was lower than average.  
380 During this period, Reco was strongly reduced (Suppl. Mat. S3c), possibly as consequence of  
381 summer drought. This was not in line with the higher sensitivity of GPP than of Reco to soil  
382 water stress, as evidenced during the 2003 hot drought (Granier et al., 2007). A similar report  
383 of 2018 higher than average NEP and GPP owing to enhanced spring carbon uptake, followed by  
384 close-to-average summer values has been reported in a Czech floodplain deciduous forest (Kowalska  
385 et al., 2020). More generally, the analysis of an ensemble of DGVM simulations and the FLUX-  
386 COM products (i.e. fluxes simulated by machine-learning techniques) over central Europe showed  
387 a seasonal (summer) influence of the 2018 heat and drought on carbon fluxes, but little to no  
388 influence on carbon fluxes at the annual scale (Bastos et al., 2020), nor on stem growth (Salomón  
389 et al., 2022). This contrasted with reports of negative annual carbon uptake anomalies evidenced  
390 in Northern Europe (Lindroth et al., 2020).

391 **Accuracy of the SWHC estimate.** We estimated SWHC to reach  $390 \pm 17$  mm at FR-  
392 Fon. This value was the 99.93<sup>th</sup> percentile of the distribution of SWHC values estimated with  
393 pedotransfer functions integrated down to 1-meter for French forests or oak stands (i.e. the same  
394 percentile for both distributions, Fig.6a). It was also very high when compared to estimates  
395 published at other sites, at which roots have been evidenced to go deeper than 1 meter (e.g. 165  
396 mm for a 200 cm root exploration depth in an oak stand in Bréda et al., 1995, maximum of 186 mm  
397 over 16 European forest sites with soils reaching depths down to 160 cm in Granier et al., 2007, see  
398 also De La Motte et al., 2020). However, SWHC values similar to, or even higher than our estimate  
399 of 390 mm have been published for temperate forests (e.g. 338 mm for the Hesse Beech forest in  
400 North-Eastern France, De La Motte et al., 2020, or 450 mm for a mixed Beech-Oak forest near  
401 Louvain-la-Neuve in Belgium, De Wergifosse et al., 2020). The value of 390 mm for SWHC was  
402 1.9 times higher than the database estimate of 207 mm for the FR-Fon grid point (Badeau et al.,  
403 2010). It is noticeable that the latter estimate was obtained from the integration of pedo-transfer  
404 functions over a soil depth of 112 cm, far lower than the actual root exploration depth at FR-Fon

405 (Suppl. Mat. S1). If considering a soil depth of 112 cm, we would estimate a SWHC of 191 mm  
406 based on our SWC measurements (integration of SWHC data per soil layers displayed in Suppl.  
407 Mat. S4). From this, we conclude (1) that our estimate of SWHC is conservative, meaning that  
408 deriving FC and PWP from SWC data (Suppl. Mat. S4) yielded similar (actually, slightly lower)  
409 values of SWHC than obtained from pedo-transfer functions (Badeau et al., 2010); (2) that what  
410 makes the SWHC of FR-Fon forest so high as compared to Badeau et al. (2010) grid point estimate  
411 is the difference of root exploration depth. Contrasting with the 112 cm-depth estimate of Badeau  
412 et al. (2010), our analysis of SWC data suggest that roots can actually extract water at least down  
413 to -300 cm at FR-Fon (Fig.4), which is supported by the observation of roots down to -300 and  
414 even -400 cm on one soil core taken at the site (Suppl. Mat S1).

415 Actually, we consider the 390-mm value as a lower-bound estimate for SWHC at FR-Fon.  
416 Indeed, we estimated this value on the basis of SWC measurements recorded during the dry 2018  
417 summer. While we are confident that our estimates of water content at field capacity were reliable,  
418 we may have underestimated the values of the wilting point (Suppl. Mat. S4), particularly for  
419 the soil layers below 100-cm depth that may have remained above the wilting point during this  
420 dry episode (note the decreasing trend of SWHC with depth below 100-cm in (Suppl. Mat. S4a).  
421 A body of evidence further supports this hypothesis: (i) our calculation of Root Water Uptake  
422 (RWU) is slightly lower than the ETR flux measured by eddy covariance (Fig.3). Yet, the latter  
423 is possibly underestimated in relation with the 18% lack of energy balance closure at the FR-Fon  
424 site. Had we increased ETR by 18% to close the energy balance, our current estimate of RWU  
425 would have more neatly lagged behind ETR. (ii) We observe that even at low REW ( $REW < 0.25$ ,  
426 red curve on Fig.5c), the canopy conductance remains relatively high. For instance Granier and  
427 Bréda (1996) (their Fig.1), report in a sessile oak stand values of canopy conductance ( $G_{can,max}$ )  
428 of  $1 \text{ cm s}^{-1}$  ( $= 0.41 \text{ mol m}^{-2} \text{ s}^{-1}$ ) under high water supply at  $VPD = 1 \text{ kPa}$ , comparable to our  
429 estimates of  $0.50 \text{ mol m}^{-2} \text{ s}^{-1}$  at FR-Fon (Fig.5c and e). Their value of  $G_{can}$  decreases to 60% of  
430  $G_{can,max}$  for  $REW = 0.2$  (Fig.2 in Granier and Bréda, 1996). In our case, we estimated that  $G_{can}$   
431 decreased to 63% of its maximum value (0.33 as compared to 0.52, Fig.5e) for  $REW = 0.1$ , pointing  
432 to a possible underestimation of REW that would stem from the underestimation of SWHC.

433 **Temporal pattern of RWU extraction along the soil profile.** The *rootwater* algorithm  
434 (Jackisch and Mälicke, 2020) fits a model to the daily variations of SWC in a given soil layer  
435 to calculate root water uptake. In the original publication, the authors consider a model fit  
436 of  $NSE > 0.5$  as indicative of most reliable RWU estimates (Jackisch et al., 2020). Our RWU  
437 calculations did not always meet this criterion, with some values of  $NSE < 0.5$  notably in early  
438 summer (before DoY 120 in 2017, or DoY 170 in 2018) and late summer (after DoY 220 in 2018)  
439 (Fig.3), meaning that processes other than root water uptake (i.e. water percolation, capillary  
440 rise) may intervene. Yet we are confident that our calculations of RWU, and their distribution  
441 among soil layers are representative of the actual uptake of water by roots, not only because  
442 RWU integrated over 0-300 cm matched the canopy transpiration flux (Fig.3) but also because  
443 the algorithm achieved model fits with  $NSE > 0.5$  at times when the deepest layers (150-300 cm)  
444 contributed a large amount of RWU (e.g. DoY 160-220 in 2017 and up to DoY 220 in 2018, Fig.4).  
445 Our calculations of root water uptake (RWU) showed that deep soil layers (i.e. below 150 cm)  
446 provisioned some water for canopy transpiration early during the leafy season, from DoY 150 (end  
447 of May) in 2017 and DoY 130 (mid-May) in 2018 (Fig.4). This contribution increased substantially,  
448 up to achieving 50% of the water uptaken for transpiration over DoY 180-220 in 2017, and even  
449 60% over DoY 210-260 in 2018 (Fig.4). A similar pattern of increasing contributions of deep soil  
450 layers to water provision for tree transpiration has already been reported (e.g. Bréda et al., 1995  
451 in an oak site, Bréda et al., 2002 in an ash forest). It is however not systematic and, for instance,  
452 a regular, not increasing, and minimal contribution of soil layers below 170 cm depth was reported  
453 in a Beech forest along a mild summer in Germany (Jackisch et al., 2020).

454 Interestingly, Bréda et al., 1995 reported, as we do, variations of SWC in soil layers located  
455 below the known root depth (reaching -200 cm in their study). We notice here that significant  
456 variations of SWC were observed at a depth of 3 meters (Fig.2b), i.e. 150 cm below the root  
457 depth established from root counting profiles made at our site (Suppl. Mat. S1). Yet, the root  
458 profile did not "close" at -150 cm at FR-Fon, and we found punctual evidence (from one soil core  
459 of 5.5-m length) that roots can actually grow down to -300 cm, and even -400 cm at this site.  
460 These observations were coherent with rooting depth of -200 cm, which are frequently reported in

461 *Quercus petraea* (Bréda et al., 1995; Lebourgeois and Jabiol, 2002) and we notice that that fine  
462 roots down to -400 cm have already been reported in *Quercus robur* (Lucot and Bruckert, 1992).

463 **Underestimating SWHC yields substantial errors in the simulation of the forest pro-**  
464 **ductivity.** Predicting the effects of current and future water stress on the functioning and distri-  
465 bution of forests is one of the key issues in ecological research. A variety of mechanistic models can  
466 be used to this aim, with some hypothesizing the forest vulnerability to rely foremost on its carbon  
467 balance (e.g. Dufrêne et al., 2005), some others simulating the integrity of the plant hydraulics  
468 (Cochard et al., 2021), and some integrating both (Davi and Cailleret, 2017; Naudts et al., 2015).  
469 Whatever the model type, it requires an accurate estimate of the amount of soil water that can  
470 be used by trees. Several papers have pointed recently the role of "deep" water reserves as key  
471 to sustain ecosystem functioning (McCormick et al., 2021; Fan et al., 2017; Carrière et al., 2020).  
472 We showed that using a SWHC estimate of 390 mm, as opposed to 207 mm as predicted by a ref-  
473 erence soil database, impacts strongly the simulation of GPP in the CASTANEA model (Fig.6c).  
474 CASTANEA is a "carbon-centric", still sensitive to the soil water balance through a modulation  
475 of the stomatal conductance vs. assimilation relation (Dufrêne et al., 2005). This model is not  
476 able to simulate the degree of xylem embolism, expected to increase as climate warms and dries  
477 (Cochard et al., 2021). Running a hydraulic-enabled model such as SUREAU (Cochard et al.,  
478 2021) or MAESPA (Duursma and Medlyn, 2012) at FR-Fon would quantify to what extent the  
479 deep-component of SWHC (i.e. the extra  $390-207=183$  mm of soil water reserve evidenced in this  
480 paper) helps mitigating the expected increase of embolism, and probability of death of trees in a  
481 warmer and drier climate.

## 482 **Conclusions and perspectives.**

483 We evidenced that the FR-Fon oak forest can tap at least 390 mm of water from the soil. This  
484 is a large amount for a temperate forest, as compared to published estimates of SWHC based on  
485 measurements (Bréda et al., 1995; De La Motte et al., 2020) or the modelling (Granier et al., 2007)  
486 of the soil water balance. This value is 1.9 times higher than the estimate of SWHC (= 207 mm)  
487 retrieved for the FR-Fon grid point in the French consensus soil database (Badeau et al., 2010),  
488 which is used in modelling studies predicting the future of French forests (Cheaib et al., 2012). Yet,  
489 several papers pointed recently the role of "deep" water in provisioning water to sustain ecosystem  
490 functioning, particularly during drought periods as the one encountered at FR-Fon in 2018. The  
491 monitoring of soil water has generally received little attention at flux measurements sites, with  
492 measurements conducted at most sites over shallow depths (typically down to 30-50 cm, Novick  
493 et al., 2016). For instance, the ICOS-network protocol states "the minimum depth of the [...]   
494 SWC profiles is set to 1 m. If limited by the presence of the bedrock or a water-impermeable layer,  
495 the profiles can be less deep" (Op De Beeck et al., 2018). Evidence is accumulating (our results  
496 and e.g. McCormick et al., 2021; Carrière et al., 2020) that water from deep soil layers can be  
497 extracted by trees in many situations, even in the presence of a "bedrock or water-impermeable  
498 layer", and that the SWHC has so far been generally largely underestimated in forests (Fig.6a),  
499 at least locally. Hence we stress here that the setup proposed by Op De Beeck et al. (2018) should  
500 be considered a minimum. SWC measurements conducted over too shallow depths will overlook  
501 the provisioning of water for canopy evapotranspiration by deeper layers. The contribution of  
502 these deep layers will probably increase as drought become more frequent and intense with climate  
503 change. While installing probes deep in the soil can be difficult, or even not practicable for some  
504 rocky sites, indirect methods such as electrical resistivity tomography (e.g. Carrière et al., 2020)  
505 are promising for evaluating the rooting depth and getting improved, higher estimates of SWHC.  
506 Beyond the documentation of SWHC at particular sites, we need more accurate maps of SWHC  
507 in order to improve the simulation of the functioning and vulnerability of forests under climate  
508 change.

## 509 **Acknowledgements**

510 We thank Augusto Zanella and Cécile Quantin for their contributions in the description of soil  
511 cores, Kamel Soudani and Eric Dufrêne for insightful discussions and their critical readings of the  
512 manuscript, Claude Doussan for discussing with us questions relative to the role of capillarity,  
513 and students Annaëlle Desgrippes and Jocelyn Ragu for their contribution in the acquisition of  
514 root distribution data. IC acknowledges funding by the ANR under the "Investissements d'avenir"  
515 programme with the reference ANR-16-CONV-0003 (CLAND).

## 516 **Authors contributions**

517 ND, JM and DB designed the research; DB, AM and GV collected the data; JM, ND and DB  
518 analysed the field data; CF did the model simulations; CF and ND analyzed the model simulations;  
519 JM, ND and DB wrote a first working paper; ND wrote the final version of the manuscript with  
520 significant inputs from MJ, IC, CF and SB.

## References

- Asner, G. P., Scurlock, J. M., and Hicke, J. A. (2003). Global synthesis of leaf area index observations: Implications for ecological and remote sensing studies. *Global Ecology and Biogeography*, 12(3):191–205.
- Badeau, V. V., Dupouey, J.-L., Cluzeau, C., Drapier, J., and Le Bas, C. (2010). Climate change and the biogeography of French tree species: first results and perspectives. In *Forests, Carbon Cycle and Climate Change*, Update Sciences and Technologies, pages 231–252. Editions Quae.
- Baldocchi, D. (2008). 'Breathing' of the terrestrial biosphere: Lessons learned from a global network of carbon dioxide flux measurement systems. *Australian Journal of Botany*, 56(1):1–26.
- Baldocchi, D. and Peñuelas, J. (2019). The physics and ecology of mining carbon dioxide from the atmosphere by ecosystems. *Global Change Biology*, 25(4):1191–1197.
- Bastos, A., Fu, Z., Ciais, P., Friedlingstein, P., Sitch, S., Pongratz, J., Weber, U., Reichstein, M., Anthoni, P., Arneth, A., Haverd, V., Jain, A., Joetzjer, E., Knauer, J., Lienert, S., Loughran, T., McGuire, P. C., Obermeier, W., Padrón, R. S., Shi, H., Tian, H., Viovy, N., and Zaehle, S. (2020). Impacts of extreme summers on European ecosystems: A comparative analysis of 2003, 2010 and 2018: European extreme summers and the C-cycle. *Philosophical Transactions of the Royal Society B: Biological Sciences*, 375(1810).
- Bréda, N., Granier, A., Barataud, F., and Moyne, C. (1995). Soil water dynamics in an oak stand - I. Soil moisture, water potentials and water uptake by roots. *Plant and Soil*, 172(1):17–27.
- Bréda, N., Lefèvre, Y., and Badeau, V. (2002). Forest soil extractable water: Specificity and estimation. *Houille Blanche*, 88(3):24–32.
- Burba, G. G., McDermitt, D. K., Grelle, A., Anderson, D. J., and Xu, L. (2008). Addressing the influence of instrument surface heat exchange on the measurements of CO<sub>2</sub> flux from open-path gas analyzers. *Global Change Biology*, 14(8):1854–1876.

545 Caldwell, M. M., Dawson, T. E., and Richards, J. H. (1998). Hydraulic lift: Consequences of water  
546 efflux from the roots of plants. *Oecologia*, 113(2):151–161.

547 Carrière, S. D., Martin-StPaul, N. K., Cakpo, C. B., Patris, N., Gillon, M., Chalikakis, K., Doussan,  
548 C., Oliosio, A., Babic, M., Jouineau, A., Simioni, G., and Davi, H. (2020). The role of deep vadose  
549 zone water in tree transpiration during drought periods in karst settings – Insights from isotopic  
550 tracing and leaf water potential. *Science of the Total Environment*, 699.

551 Cheaib, A., Badeau, V., Boe, J., Chuine, I., Delire, C., Dufrière, E., François, C., Gritti, E. S.,  
552 Legay, M., Pagé, C., Thuiller, W., Viovy, N., and Leadley, P. (2012). Climate change impacts on  
553 tree ranges: Model intercomparison facilitates understanding and quantification of uncertainty.  
554 *Ecology Letters*, 15(6):533–544.

555 Christina, M., Nouvellon, Y., Laclau, J. P., Stape, J. L., Bouillet, J. P., Lambais, G. R., and  
556 le Maire, G. (2017). Importance of deep water uptake in tropical eucalypt forest. *Functional*  
557 *Ecology*, 31(2):509–519.

558 Cochard, H., Pimont, F., Ruffault, J., and Martin-StPaul, N. (2021). SurEau: a mechanistic model  
559 of plant water relations under extreme drought. *Annals of Forest Science*, 78(2).

560 Cramer, M. D., Hawkins, H. J., and Verboom, G. A. (2009). The importance of nutritional  
561 regulation of plant water flux. *Oecologia*, 161(1):15–24.

562 Davi, H. and Cailleret, M. (2017). Assessing drought-driven mortality trees with physiological  
563 process-based models. *Agricultural and Forest Meteorology*, 232:279–290.

564 De La Motte, L. G., Beauclaire, Q., Heinesch, B., Cuntz, M., Foltýnová, L., Šigut, L., Kowalska,  
565 N., Manca, G., Ballarin, I. G., Vincke, C., Roland, M., Ibrom, A., Lousteau, D., Siebicke, L.,  
566 Neiryink, J., and Longdoz, B. (2020). Non-stomatal processes reduce gross primary productiv-  
567 ity in temperate forest ecosystems during severe edaphic drought: Edaphic drought in forest  
568 ecosystems. *Philosophical Transactions of the Royal Society B: Biological Sciences*, 375(1810).

569 De Wergifosse, L., André, F., Beudez, N., De Coligny, F., Goosse, H., Jonard, F., Ponette, Q.,  
570 Titeux, H., Vincke, C., and Jonard, M. (2020). HETEROFOR 1.0: A spatially explicit model

571 for exploring the response of structurally complex forests to uncertain future conditions-Part 2:  
572 Phenology and water cycle. *Geoscientific Model Development*, 13(3):1459–1498.

573 Delpierre, N., Berveiller, D., Granda, E., and Dufrêne, E. (2016). Wood phenology, not carbon  
574 input, controls the interannual variability of wood growth in a temperate oak forest. *New*  
575 *Phytologist*, 210(2):459–470.

576 Delpierre, N., Soudani, K., François, C., Le Maire, G., Bernhofer, C., Kutsch, W., Misson, L.,  
577 Rambal, S., Vesala, T., and Dufrêne, E. (2012). Quantifying the influence of climate and  
578 biological drivers on the interannual variability of carbon exchanges in European forests through  
579 process-based modelling. *Agricultural and Forest Meteorology*, 154-155:99–112.

580 Dufrêne, E., Davi, H., François, C., Maire, G. L., Dantec, V. L., and Granier, a. (2005). Modelling  
581 carbon and water cycles in a beech forest. *Ecological Modelling*, 185(2-4):407–436.

582 Duursma, R. A. and Medlyn, B. E. (2012). MAESPA: A model to study interactions between  
583 water limitation, environmental drivers and vegetation function at tree and stand levels, with  
584 an example application to [CO<sub>2</sub>] × drought interactions. *Geoscientific Model Development*,  
585 5(4):919–940.

586 Eagleson, P. S. (1982). Ecological optimality in water-limited natural soil-vegetation systems: 1.  
587 Theory and hypothesis. *Water Resources Research*, 18(2):325–340.

588 Fan, Y., Miguez-Macho, G., Jobbágy, E. G., Jackson, R. B., and Otero-Casal, C. (2017). Hydrologic  
589 regulation of plant rooting depth. *Proceedings of the National Academy of Sciences of the United*  
590 *States of America*, 114(40):10572–10577.

591 Germon, A., Laclau, J. P., Robin, A., and Jourdan, C. (2020). Tamm Review: Deep fine roots in  
592 forest ecosystems: Why dig deeper? *Forest Ecology and Management*, 466(4):118135.

593 Granier, A. and Bréda, N. (1996). Modelling canopy conductance and stand transpiration of an  
594 oak forest from sap flow measurements. *Annales des Sciences Forestières*, 53(2-3):537–546.

595 Granier, A., Bréda, N., Biron, P., and Villette, S. (1999). A lumped water balance model to  
596 evaluate duration and intensity of drought constraints in forest stands. *Ecological Modelling*,  
597 116(2-3):269–283.

598 Granier, A., Reichstein, M., Bréda, N., Janssens, I. A., Falge, E., Ciais, P., Grünwald, T., Aubinet,  
599 M., Berbigier, P., Bernhofer, C., Buchmann, N., Facini, O., Grassi, G., Heinesch, B., Ilvesniemi,  
600 H., Keronen, P., Knohl, A., Köstner, B., Lagergren, F., Lindroth, A., Longdoz, B., Loustau, D.,  
601 Mateus, J., Montagnani, L., Nys, C., Moors, E., Papale, D., Peiffer, M., Pilegaard, K., Pita,  
602 G., Pumpanen, J., Rambal, S., Rebmann, C., Rodrigues, A., Seufert, G., Tenhunen, J., Vesala,  
603 T., and Wang, Q. (2007). Evidence for soil water control on carbon and water dynamics in  
604 European forests during the extremely dry year: 2003. *Agricultural and Forest Meteorology*,  
605 143(1-2):123–145.

606 Grossiord, C., Buckley, T. N., Cernusak, L. A., Novick, K. A., Poulter, B., Siegwolf, R. T., Sperry,  
607 J. S., and McDowell, N. G. (2020). Plant responses to rising vapor pressure deficit. *New*  
608 *Phytologist*, 226(6):1550–1566.

609 Guderle, M. and Hildebrandt, A. (2015). Using measured soil water contents to estimate evapo-  
610 transpiration and root water uptake profiles-a comparative study. *Hydrology and Earth System*  
611 *Sciences*, 19(1):409–425.

612 Guillemot, J., Francois, C., Hmimina, G., Dufrêne, E., Martin-StPaul, N. K., Soudani, K., Marie,  
613 G., Ourcival, J. M., and Delpierre, N. (2017). Environmental control of carbon allocation matters  
614 for modelling forest growth. *New Phytologist*, 214(1):180–193.

615 Hsiao, T. C., Acevedo, E., Fereres, E., and Henderson, D. W. (1976). Stress metabolism - Wa-  
616 ter stress, growth and osmotic adjustment. *Philosophical transactions of the Royal Society of*  
617 *London. Series B, Biological sciences*, 273:479–500.

618 Hupet, F., Lambot, S., Javaux, M., and Vanclooster, M. (2002). On the identification of macro-  
619 scopic root water uptake parameters from soil water content observations. *Water Resources*  
620 *Research*, 38(12):1300.

- 621 Ishikawa, C. M. and Bledsoe, C. S. (2000). Seasonal and diurnal patterns of soil water potential  
622 in the rhizosphere of blue oaks: Evidence for hydraulic lift. *Oecologia*, 125(4):459–465.
- 623 IUSS Working Group WRB (2015). *World Reference Base for Soil Resources 2014, update 2015*.  
624 *International soil classification system for naming soils and creating legends for soil maps*. Num-  
625 ber 106. FAO, Rome.
- 626 Jackisch, C., Knoblauch, S., Blume, T., Zehe, E., and Hassler, S. K. (2020). Estimates of tree root  
627 water uptake from soil moisture profile dynamics. *Biogeosciences*, 17(22):5787–5808.
- 628 Jackisch, C. and Mälicke, M. (2020). cojaco/rootwater: Rootwater with updated Astral references  
629 (v0.3).
- 630 Jackson, R. B., Canadell, J., Ehleringer, J. R., Mooney, H. A., Sala, O. E., and Schulze, E. D.  
631 (1996). A global analysis of root distributions for terrestrial biomes. *Oecologia*, 108(3):389–411.
- 632 Jamagne, M., Hardy, R., King, D., and Bornand, M. (1995). La base de données géographique des  
633 sols de France. *Etude et Gestion des Sols*, 2(3):153–172.
- 634 Jourdan, M., François, C., Delpierre, N., St-Paul, N. M., and Dufrêne, E. (2021). Reliable predic-  
635 tions of forest ecosystem functioning require flawless climate forcings. *Agricultural and Forest*  
636 *Meteorology*, 311(12):108703.
- 637 Kowalska, N., Šigut, L., Stojanović, M., Fischer, M., Kyselova, I., and Pavelka, M. (2020). Analysis  
638 of floodplain forest sensitivity to drought: Floodplain forest during drought. *Philosophical*  
639 *Transactions of the Royal Society B: Biological Sciences*, 375(1810).
- 640 Krinner, G., Viovy, N., de Noblet-Ducoudré, N., Ogée, J., Polcher, J., Friedlingstein, P., Ciais,  
641 P., Sitch, S., and Prentice, I. C. (2005). A dynamic global vegetation model for studies of the  
642 coupled atmosphere-biosphere system. *Global Biogeochemical Cycles*, 19:GB 1015.
- 643 Lebourgeois, F. and Jabiol, B. (2002). Enracinements comparés du Chêne sessile, du Chêne  
644 pédonculé et du Hêtre. Réflexions sur l’autécologie des essences. *Revue forestière française*,  
645 54(1):17–42.

646 Li, Y., Fuchs, M., Cohen, S., Cohen, Y., and Wallach, R. (2002). Water uptake profile response of  
647 corn to soil moisture depletion. *Plant, Cell and Environment*, 25(4):491–500.

648 Lindroth, A., Holst, J., Linderson, M. L., Aurela, M., Biermann, T., Heliasz, M., Chi, J., Ibrom,  
649 A., Kolari, P., Klemedtsson, L., Krasnova, A., Laurila, T., Lehner, I., Lohila, A., Mammarella,  
650 I., Mölder, M., Löfvenius, M. O., Peichl, M., Pilegaard, K., Soosar, K., Vesala, T., Vestin, P.,  
651 Weslien, P., and Nilsson, M. (2020). Effects of drought and meteorological forcing on carbon  
652 and water fluxes in Nordic forests during the dry summer of 2018. *Philosophical Transactions  
653 of the Royal Society B: Biological Sciences*, 375(1810).

654 Lucot, E. and Bruckert, S. (1992). Common oak (*Quercus robur*) root system organisation devel-  
655 oped without restricting edaphic conditions - colluvial leached brown soil. *Annales des Sciences  
656 Forestieres*, 49(5):465–479.

657 Martin-StPaul, N., Delzon, S., and Cochard, H. (2017). Plant resistance to drought depends on  
658 timely stomatal closure. *Ecology Letters*, 20(11):1437–1447.

659 McCormick, E. L., Dralle, D. N., Hahm, W. J., Tune, A. K., Schmidt, L. M., Chadwick, K. D.,  
660 and Rempe, D. M. (2021). Widespread woody plant use of water stored in bedrock. *Nature*,  
661 597(7875).

662 Moncrieff, J., Clement, R., Finnigan, J., and Meyers, T. (2005). Averaging, detrending and  
663 filtering of eddy covariance time series. In *Handbook of micrometeorology*, pages 7–31. Springer  
664 Netherlands.

665 Moncrieff, J., Massheder, J., de Bruin, H., Elbers, J., Friborg, T., Heusinkveld, B., Kabat, P., Scott,  
666 S., Soegaard, H., and Verhoef, a. (1997). A system to measure surface fluxes of momentum,  
667 sensible heat, water vapour and carbon dioxide. *Journal of Hydrology*, 188-189:589–611.

668 Nash, J. E. and Sutcliffe, J. V. (1970). River flow forecasting through conceptual models part I -  
669 A discussion of principles. *Journal of Hydrology*, 10(3):282–290.

670 Naudts, K., Ryder, J., McGrath, M. J., Otto, J., Chen, Y., Valade, A., Bellasen, V., Berhongaray,  
671 G., Bönisch, G., Campioli, M., Ghattas, J., De Groote, T., Haverd, V., Kattge, J., MacBean,

672 N., Maignan, F., Merilä, P., Penuelas, J., Peylin, P., Pinty, B., Pretzsch, H., Schulze, E. D.,  
673 Solyga, D., Vuichard, N., Yan, Y., and Luysaert, S. (2015). A vertically discretised canopy  
674 description for ORCHIDEE (SVN r2290) and the modifications to the energy, water and carbon  
675 fluxes. *Geoscientific Model Development*, 8(7).

676 Nelson, J., Carvalhais, N., Cuntz, M., Delpierre, N., Knauer, J., Ogée, J., Migliavacca, M., Reich-  
677 stein, M., and Jung, M. (2018). Coupling Water and Carbon Fluxes to Constrain Estimates of  
678 Transpiration: The TEA Algorithm. *Journal of Geophysical Research: Biogeosciences*, 123(12).

679 Neumann, R. B. and Cardon, Z. G. (2012). The magnitude of hydraulic redistribution by plant  
680 roots: A review and synthesis of empirical and modeling studies. *New Phytologist*, 194(2):337–  
681 352.

682 Novick, K. A., Ficklin, D. L., Stoy, P. C., Williams, C. A., Bohrer, G., Oishi, A. C., Papuga,  
683 S. A., Blanken, P. D., Noormets, A., Sulman, B. N., Scott, R. L., Wang, L., and Phillips, R. P.  
684 (2016). The increasing importance of atmospheric demand for ecosystem water and carbon  
685 fluxes. *Nature Climate Change*, 6(11):1023–1027.

686 Op De Beeck, M., Gielen, B., Merbold, L., Ayres, E., Serrano-Ortiz, P., Acosta, M., Pavelka,  
687 M., Montagnani, L., Nilsson, M., Klemedtsson, L., Vincke, C., De Ligne, A., Moureaux, C.,  
688 Marañon-Jimenez, S., Saunders, M., Mereu, S., and Hörtnagl, L. (2018). Soil-meteorological  
689 measurements at ICOS monitoring stations in terrestrial ecosystems. *International Agrophysics*,  
690 32(4):619–631.

691 Oren, R., Sperry, J. S., Katul, G. G., Pataki, D. E., Ewers, B. E., Phillips, N., and Schäfer,  
692 K. V. (1999). Survey and synthesis of intra- and interspecific variation in stomatal sensitivity  
693 to vapour pressure deficit. *Plant, Cell and Environment*, 22(12):1515–1526.

694 Papale, D., Reichstein, M., Aubinet, M., Canfora, E., Bernhofer, C., Kutsch, W., Longdoz, B.,  
695 Rambal, S., Valentini, R., Vesala, T., and Yakir, D. (2006). Towards a standardized processing of  
696 Net Ecosystem Exchange measured with eddy covariance technique: algorithms and uncertainty  
697 estimation. *Biogeosciences*, 3(4):571–583.

698 Piedallu, C., Gégout, J. C., Bruand, A., and Seynave, I. (2011). Mapping soil water holding  
699 capacity over large areas to predict potential production of forest stands. *Geoderma*, 160(3-  
700 4):355–366.

701 Preisler, Y., Tatarinov, F., Grünzweig, J. M., Bert, D., Ogée, J., Wingate, L., Rotenberg, E.,  
702 Rohatyn, S., Her, N., Moshe, I., Klein, T., and Yakir, D. (2019). Mortality versus survival  
703 in drought-affected Aleppo pine forest depends on the extent of rock cover and soil stoniness.  
704 *Functional Ecology*, 33(5):901–912.

705 Provenzano, G., Rallo, G., and Ghazouani, H. (2016). Assessing Field and Laboratory Calibration  
706 Protocols for the Diviner 2000 Probe in a Range of Soils with Different Textures. *Journal of*  
707 *Irrigation and Drainage Engineering*, 142(2):04015040.

708 Reichstein, M., Ciais, P., Papale, D., Valentini, R., Running, S., Viovy, N., Cramer, W., Granier,  
709 A., Ogée, J., Allard, V., Aubinet, M., Bernhofer, C., Buchmann, N., Carrara, A., Grünwald,  
710 T., Heimann, M., Heinesch, B., Knohl, A., Kutsch, W., Loustau, D., Manca, G., Matteucci, G.,  
711 Miglietta, F., Ourcival, J. M., Pilegaard, K., Pumpanen, J., Rambal, S., Schaphoff, S., Seufert,  
712 G., Soussana, J. F., Sanz, M. J., Vesala, T., and Zhao, M. (2007). Reduction of ecosystem  
713 productivity and respiration during the European summer 2003 climate anomaly: A joint flux  
714 tower, remote sensing and modelling analysis. *Global Change Biology*, 13(3):634–651.

715 Reichstein, M., Falge, E., Baldocchi, D., Papale, D., Aubinet, M., Berbigier, P., Bernhofer, C.,  
716 Buchmann, N., Gilmanov, T., Granier, A., Grünwald, T., Havránková, K., Ilvesniemi, H.,  
717 Janous, D., Knohl, A., Laurila, T., Lohila, A., Loustau, D., Matteucci, G., Meyers, T., Migli-  
718 etta, F., Ourcival, J. M., Pumpanen, J., Rambal, S., Rotenberg, E., Sanz, M., Tenhunen, J.,  
719 Seufert, G., Vaccari, F., Vesala, T., Yakir, D., and Valentini, R. (2005). On the separation  
720 of net ecosystem exchange into assimilation and ecosystem respiration: Review and improved  
721 algorithm. *Global Change Biology*, 11(9):1424–1439.

722 Salomón, R. L., Peters, R. L., Zweifel, R., Sass-Klaassen, U. G., Stegehuis, A. I., Smiljanic, M.,  
723 Poyatos, R., Babst, F., Cienciala, E., Fonti, P., Lerink, B. J., Lindner, M., Martinez-Vilalta,  
724 J., Mencuccini, M., Nabuurs, G. J., van der Maaten, E., von Arx, G., Bär, A., Akhmetzyanov,

725 L., Balanzategui, D., Bellan, M., Bendix, J., Berveiller, D., Blaženec, M., Čada, V., Carraro,  
726 V., Cecchini, S., Chan, T., Conedera, M., Delpierre, N., Delzon, S., Ditmarová, , Dolezal, J.,  
727 Dufrêne, E., Edvardsson, J., Ehekircher, S., Forner, A., Frouz, J., Ganthaler, A., Gryc, V.,  
728 Güney, A., Heinrich, I., Hentschel, R., Janda, P., Ježík, M., Kahle, H. P., Knüsel, S., Krejza,  
729 J., Kuberski, L., Kučera, J., Lebourgeois, F., Mikoláš, M., Matula, R., Mayr, S., Oberhuber,  
730 W., Obojes, N., Osborne, B., Paljakka, T., Plichta, R., Rabbel, I., Rathgeber, C. B., Salmon,  
731 Y., Saunders, M., Scharnweber, T., Sitková, Z., Stangler, D. F., Stereńczak, K., Stojanović,  
732 M., Střelcová, K., Světlík, J., Svoboda, M., Tobin, B., Trotsiuk, V., Urban, J., Valladares, F.,  
733 Vavřík, H., Vejpustková, M., Walthert, L., Wilmking, M., Zin, E., Zou, J., and Steppe, K.  
734 (2022). The 2018 European heatwave led to stem dehydration but not to consistent growth  
735 reductions in forests. *Nature Communications*, 13(1):28.

736 Samaniego, L., Thober, S., Kumar, R., Wanders, N., Rakovec, O., Pan, M., Zink, M., Sheffield, J.,  
737 Wood, E. F., and Marx, A. (2018). Anthropogenic warming exacerbates European soil moisture  
738 droughts. *Nature Climate Change*, 8(5):421–426.

739 Sentek Pty Ltd (2001). CALIBRATION MANUAL For Sentek Soil Moisture Sensors Version 2.0.  
740 Technical report, Sentek Pty Ltd.

741 Soudani, K., Delpierre, N., Berveiller, D., Hmimina, G., Pontailier, J. Y., Seureau, L., Vincent,  
742 G., and Dufrêne, É. (2021). A survey of proximal methods for monitoring leaf phenology in  
743 temperate deciduous forests. *Biogeosciences*, 18(11):3391–3408.

744 Thiry, M. (2010). Le plateau de Brie à Fontaine-le-Port : géologie, géomorphologie, hydrologie et  
745 aménagement du territoire. Technical report, Association Naturaliste de la Vallée du Loing et  
746 du massif de Fontainebleau.

747 van Genuchten, M. T. (1980). A Closed-form Equation for Predicting the Hydraulic Conductivity  
748 of Unsaturated Soils. *Soil Science Society of America Journal*, 44(5):892–898.

749 Wilson, K., Goldstein, A., Falge, E., Aubinet, M., Baldocchi, D., Berbigier, P., Bernhofer, C.,  
750 Ceulemans, R., Dolman, H., Field, C., Grelle, A., Ibrom, A., Law, B. E., Kowalski, A., Meyers,

- 751 T., Moncrieff, J., Monson, R., Oechel, W., Tenhunen, J., Valentini, R., and Verma, S. (2002).  
752 Energy balance closure at FLUXNET sites. *Agricultural and Forest Meteorology*, 113(1-4):223–  
753 243.
- 754 Zuo, Q. and Zhang, R. (2002). Estimating root-water-uptake using an inverse method. *Soil Science*,  
755 167(9):561–571.